

Demonstration and characterisation of a new interferometric particle imaging configuration for bubbles

Sam Dehaeck^{1,2} and Jeroen P.A.J. van Beeck¹

¹ Von Karman Institute for Fluid Dynamics, Sint-Genesius-Rode, Belgium, vanbeeck@vki.ac.be

² Dept. of Flow, Heat and Comb. Mech., Ghent University, Gent, Belgium, dehaeck@vki.ac.be

Abstract

Extended ILIDS is introduced for measuring the diameter of bubbles under an angle close or equal to 90° with perpendicular polarisation. For this configuration two dominant frequency peaks are present in the power spectrum, which have a known frequency ratio. Since this signature is not easily reproduced by different scatterers, this configuration has an increased robustness compared to regular ILIDS. Additionally, this frequency signature was shown to be most sensitive to deviations from sphericity, making it a good detector of non-spherical bubbles. Apart from this, a detailed analysis of the different ILIDS calibration procedures revealed that the highest precision can be obtained with a two-step calibration procedure where the camera reaches focus half-way between the final ILIDS camera position and the measurement volume. Finally, measurements of the diameter of the same bubble were compared for three different techniques, i.e. backlighting, ILIDS and GPVS and these results differed by less than 1%.

1 Introduction

For measuring accurately the size distribution and void fraction of micro-bubbles, one preferably uses a non-intrusive technique, which is able to measure precisely the location and size of each bubble. A suitable technique for this is Interferometric Laser Imaging for Droplet Sizing (ILIDS) as introduced by Koenig et al. [1986], Ragucci et al. [1990] and Glover et al. [1995]. This technique is also known under various different names as IPI (Interferometric Particle Imaging) and MSI (Mie Scattering Imaging). In this technique, translucent particles are illuminated by a laser-sheet. Depending on the observation angle, one or multiple bright points (i.e. glare points) are visible on the particle surface. When these points are imaged out-focus an interference pattern will become visible with a shape that is determined by the aperture. The angular frequency of this pattern is proportional to the separating distance between the two glare points and thus to the particle diameter.

So far the development of this technique has been focused almost exclusively on measuring droplets. Nevertheless, the same principles also apply to bubbles. Niwa et al. [2000] demonstrated how bubbles could be measured with ILIDS under an observation angle of 45° . However, as was discussed in Dehaeck et al. [2005], this oblique angle reduces the allowable void fraction and is rather sensitive to misalignment and refractive index changes. Two improved configurations were also proposed; a single laser-sheet configuration under 96° and a two laser-sheet configuration under 90° . The symmetrical configuration was already demonstrated by Palero et al. [2005] while Langley and Marston [1984] have already showed that an accurate size measurement can be obtained from the interference pattern created with the single laser-sheet set-up. However, they did not use the planar arrangement typical for ILIDS and opted to stay close to the critical angle ($\pm 83^\circ$). The symmetrical configuration on the other hand has a high demand on the coherence length of the laser.

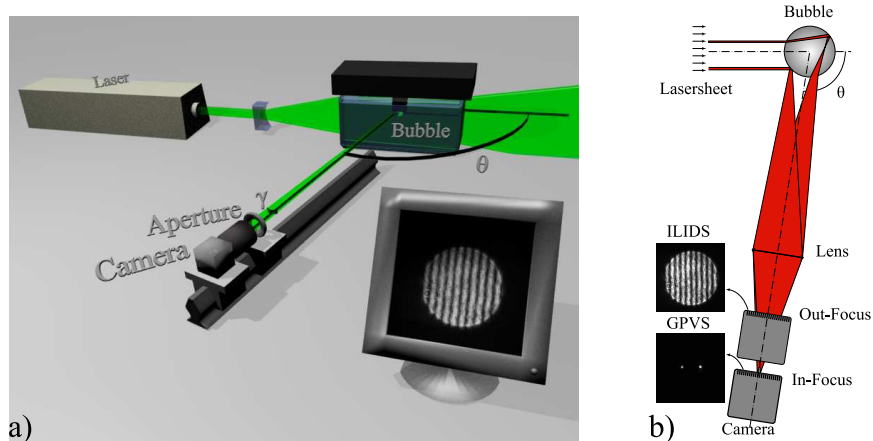


Figure 1: a) Experimental configuration to obtain a stable bubble b) Sketch explaining GPVS-ILIDS

In this article, we will follow the ideas proposed in Dehaeck et al. [2004], and use a configuration where multiple glare points are visible. The relative position of these glare points can then be used to obtain a more robust measurement. An explanation of this configuration is given in Section 3. This is followed by the derivation of the necessary formulas for ILIDS and a detailed analysis of the different possible calibration procedures together with some recommendations. Finally, a direct comparison of measurements on the same bubble with backlighting, GPVS and ILIDS will conclude the article.

2 Experimental Set-Up

In order to demonstrate the possibility to measure the correct bubble diameter with the new ILIDS configuration, a comparison with backlighting and GPVS was performed. In the absence of a monodisperse bubble generator, a stable bubble was produced and measured with both techniques sequentially. This was achieved with the configuration shown in Figure 1a for ILIDS. A reservoir filled with silicone oil ($n=1,403$) is used and the bubble is simply kept in place by a wooden block. Naturally, this obstruction creates a non-spherical bubble in a vertical plane. However, with GPVS and ILIDS the diameter of the bubble is measured in a horizontal plane. Since all forces in this plane are symmetrical, the bubble is spherical as far as ILIDS is concerned.

3 Extended ILIDS

In Dehaeck et al. [2004], an angle close to 90° is suggested where $N=1$ and $N=3$ are equally intense for parallel polarised light. In the current situation this angle would be 105° . However, much better results are obtained with perpendicular polarisation compared to parallel for the same settings, as can be seen in Figure 2a and 2b. This was surprising since for perpendicular polarisation the ray coming from external reflection is approximately 8 times more intense than the ray from internal reflection! Theoretically this leads to a visibility of the fringes of only 0,68 compared to 1 for parallel polarisation. A simulation of both cases with a raytracing program (only $N=1$ and $N=3$ are considered) for the current set-up is shown in Figure 2c. This shows qualitatively the same results as the two images. For perpendicular polarisation, both the absolute size of the fringes and the average intensity are larger compared to parallel polarisation. Now, to come back to the lower visibility. This is a theoretical concept, which only has a real meaning if one is able to map the maximum scattered intensity to the maximum gray-scale value of the camera. Looking at Figure 2c, one can see that if

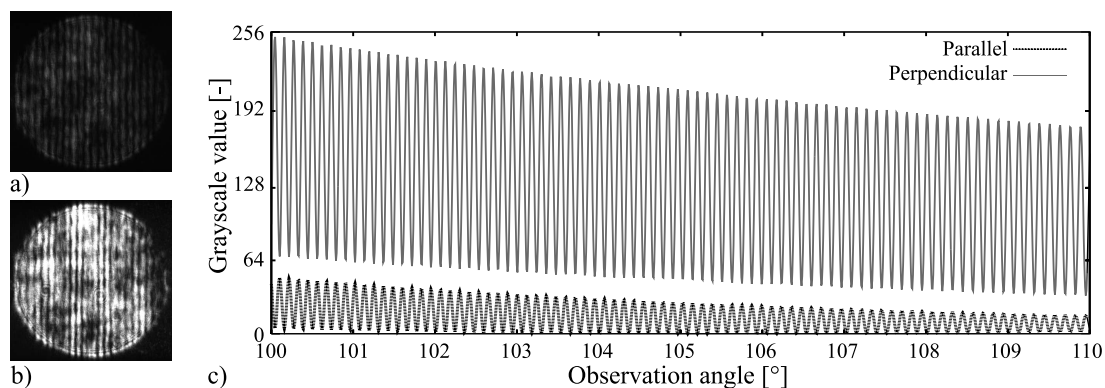


Figure 2: a) ILIDS image under parallel polarisation b) perpendicular polarisation with same settings c) Theoretical interference pattern reated by $N=1$ and $N=3$ for parallel and perpendicular polarisation

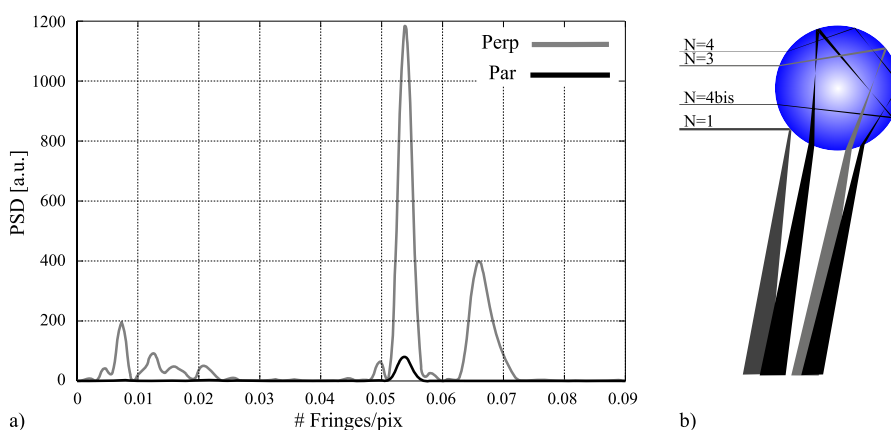


Figure 3: a) FFT result of two images from Figure 2 b) Illustration of higher order glare points

the laser intensity could be increased, it would be possible to obtain fringes going from a gray-scale value of 0 to 256 under parallel polarisation, while this is not possible with perpendicular polarisation due to the offset. However, since the scattered intensity is rather low for the current scattering angle, this increase in intensity is not always achievable. This was noticed when performing measurements on moving bubbles in water; measuring with a continuous 2 W Ar-ion laser was not possible with parallel polarisation due to the restriction on the shutter time to freeze the image but posed no problem under perpendicular polarisation.

When analysing both images, the power spectrum from Figure 3a is obtained. Here, one can see that in both cases there is a peak detected at approximately 0,054 fringes/pix but the perpendicular peak is approximately 15 times larger! This peak corresponds to the interference pattern generated by $N=1$ and $N=3$ and demonstrates once again the superiority of the perpendicular polarisation for the same optical settings. However, for this case, there clearly is another frequency present at approximately 0,066 fringes/pix, which is not visible in the parallel case. Inspection of the intensity versus observation angle plot (not shown) revealed that the next bright glare point corresponds to $N=4$ (shown in Figure 3b). This glare point is 11 times less intense than $N=3$ but apparently, the interference pattern created by $N=1$ and this glare point is still visible. The glare point corresponding to $N=4bis$ is 5 times smaller still than $N=4$ and results in less visible peaks. This appearance of multiple peaks in the frequency analysis which correspond to different glare points is very similar to extended GPVS by Dehaeck et al. [2004]. Following their ideas, one can now try to use the relative position of this secondary peak, since it is independent of the bubble diameter, to increase the robustness of the mea-

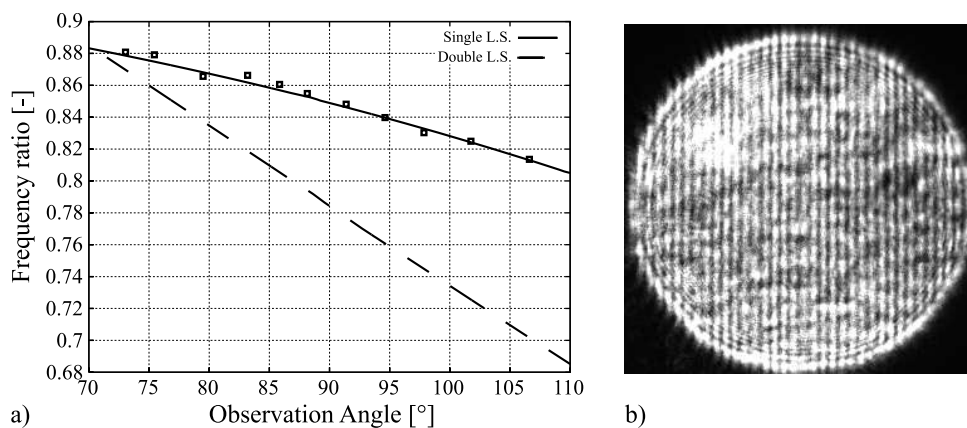


Figure 4: a) Frequency peak ratio versus observation angle b) Extended ILIDS under 90°

surement. Thus, instead of simply assuming that the highest peak in the FFT-result corresponds to the interference pattern of $N=1$ and $N=3$, one can search for two peaks with a fixed ratio. This will make the measurement more robust since it is less likely that this signature will appear in the absence of a bubble. While the basic principle of extended GPVS and extended ILIDS is the same, the used glare points are different. In extended GPVS the third glare point is coming from external reflection of a second laser-sheet that has an opposite direction, whereas for extended ILIDS only a single laser-sheet is needed! Next to several practical advantages, this configuration also poses lower demands on the required coherence length of the laser. This implies that one can perform extended ILIDS with a regular Nd-Yag laser which only has a coherence length of several centimeter. While Palero et al. [2005] have showed that this is also possible with a two-laser-sheet configuration, the size of their measurement reservoir (1,5 cm) had to remain small in order to maintain the coherence.

Although we assumed that the extra peak corresponds to the interference pattern of $N=1$ and $N=4$, we did not yet prove it. This is attempted in Figure 4a. In this graph the ratio of both frequency peaks is plotted versus the observation angle. The open squares represent experimental values that were obtained by placing the rail in Figure 1a parallel to the laser-sheet at a certain distance and for different positions of the camera. The full line represents our hypothesis while the dashed line corresponds to the variation one could expect for two laser-sheets and a second externally reflected glare point, i.e. the set-up for extended GPVS. This graph clearly shows that the second frequency is due to $N=4$ and we obtain a close fitting of experiments and theory.

Another side-effect of the use of perpendicular light instead of parallel light, is the observation that it is not necessary to use an angle of 105°. This opens the road to use an angle closer to 90°. Figure 2c even suggests that both the absolute fringe and main intensity increase for angles closer to 90° (due to the nearness of the critical angle..). An example image with extended ILIDS under 90° is shown in Figure 4b, demonstrating the feasibility of this technique under 90°.

In order to verify if we could use the frequency signature to extract information concerning the refractive index and the non-sphericity of the bubble as has been done in extended GPVS, its variation in function of several parameters is plotted in Figure 5. In 5a, the variation with respect to the observation angle is shown again, both for bubbles in silicone and for bubbles in water. As you can see, the ratio is not really sensitive to the refractive index. This is confirmed by Figure 5b, where the variation with the refractive index is plotted. Especially for an observation angle of 90°, the frequency ratio is insensitive to variations in the refractive index. Finally Figure 5c shows the variation with the tilt angle for an ellipsoidal bubble with an aspect ratio of 0,9 observed under 90° in water. As with extended GPVS, the ratio changes considerably for a given aspect ratio depending on the tilt angle of the bubble. Now, how can we use these graphs. The observation angle will in general not vary

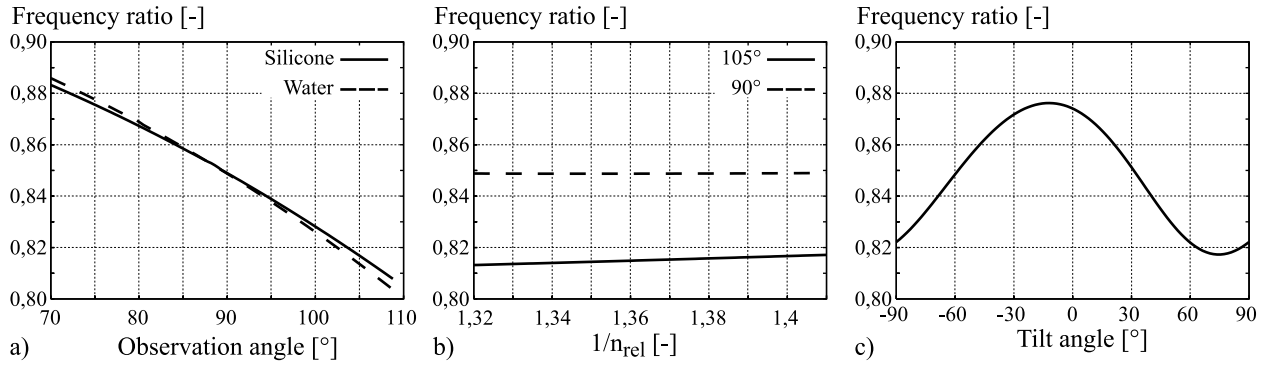


Figure 5: Variation of the frequency signature with respect to a) observation angle b) refractive index c) tilt angle for an ellipsoidal bubble with an aspect ratio of 0,9

from 70° to 110° across our field of view but this will be closer to 1°. This corresponds to a change in the frequency ratio of only 0,17%. Similarly, changes in refractive index have almost no influence. Therefore, the only important parameter is the non-sphericity of the bubble. Thus, the frequency ratio can be used as a non-sphericity detector! However, as is shown in Figure 5c, the detected ratio can always reach the spherical ratio for a certain tilt angle no matter the aspect ratio. Unfortunately, contrary to extended GPVS, the conversion factor in this case for the ellipse is not virtually equal to the spherical conversion factor and would lead to an error of 5% for an aspect ratio of 0,9 in water under 90°. Thus, although it is not flawless, most of the non-spherical bubbles will be detected correctly.

4 Formula

The formulas necessary to perform ILIDS will be derived yet again in this article. This is mainly because we wish to unify the formulas for GPVS and ILIDS. Now, the interference pattern coming from two glare points is analogous to the one observed from two point sources (as in Young's experiment). The angular fringe spacing for such a configuration can be found in Hecht [1990] and is given by:

$$\Delta\varphi = \frac{\lambda}{m_{medium}\delta}$$

In this formula $\Delta\varphi$ is the angular fringe spacing, λ is the wavelength of the laser, δ is the distance between the two glare points and m_{medium} is the refractive index of the surrounding medium. The choice of this refractive index is not so straightforward in the case of air bubbles in a water tank. Semidetnov and Tropea [2004] suggest the following approach. First, calculate the angular fringe spacing in water ($m_{medium} = 1,33$) and afterwards, apply the following correction:

$$\Delta\varphi_{air} = \Delta\varphi_{water} m_{water} \frac{\sin(\theta_{water})}{\sin(\theta_{air})}$$

Closer examination of this correction reveals that the refractive index of water is eliminated and that the glare point spacing is reduced due to the deflection at the wall. Thus, what follows is simply the angular fringe spacing in air from the reduced glare point separation:

$$D_{bubble} = \frac{\lambda\alpha_{air}}{\Delta\varphi_{air}}$$

Here, α_{air} is the conversion factor to calculate the bubble diameter (D_{bubble}) from the observed glare point separation in air as would be used by GPVS (Dehaeck et al. [2004]). For GPVS, the bubble diameter is obtained through the formula $D_{bubble} = M\alpha_{air}\Delta$, where M is the optical magnification and Δ is the glare point separation. So both formulas are indeed very close and the value α_{air} can be reused across the techniques. Now, the value α_{air} can be obtained analytically for spherical bubbles but for ellipsoidal shapes a numerical ray-tracing approach is easier. Alternatively, this value can also be obtained from Lorenz-Mie calculations as done by Pan et al. [2005]. A second reason for not replacing this factor with its analytic equivalent is that the formula in this stage is completely implementation agnostic. The same formula can be used for different combinations of glare points and even for water droplets in air since this only influences the value of α_{air} . A detailed uncertainty analysis was already performed for this variable in Dehaeck et al. [2005] and will not be repeated here.

While α_{air} is calculated from the optical configuration, the fringe spacing $\Delta\varphi_{air}$ has to be extracted *in radian* from the ILIDS images. This is not straightforward however and there are different approaches to achieve this. Most of these techniques separate this in two sub-tasks; a) measure the fringe spacing in pixels and b) multiply this value with a 'calibration' value to convert this from pixels to radian. Four different approaches will be discussed in the next sections.

5 Calibration

5.1 Fringe Counting

This is the oldest and also the easiest method for performing ILIDS measurements that was already used by Ragucci et al. [1990]. Note that in this approach there is no clear distinction between a measurement of the fringe spacing in pixels and a calibration of the amount of radian per pixel. Instead, only two variables need to be known, the collecting angle γ and the amount of fringes inside the ILIDS disc N_f . The collecting angle γ is equal to the total amount of radian that is gathered by the lens (see Figure 1a). Since this range of angles is mapped on the out-focus disc, one can calculate the angular fringe spacing by dividing the total amount of mapped radians by the total amount of fringes. Thus, we have:

$$\Delta\varphi = \frac{\gamma}{N_f}$$

The largest uncertainty associated with this measurement procedure is definitely due to the need to count the amount of fringes. By its very nature this is limited to integral numbers yielding an uncertainty of ± 1 . For a target uncertainty of 2 %, at least 50 fringes should be imaged. To this end, a typical disc size should already have a diameter of 200 pixels, which would only allow a very small amount of bubbles to be imaged at the same time! In addition, when several discs overlap, a good measurement is likely to be impossible, reducing the allowable concentration even further.

5.2 Experimental Calibration

Since an interference pattern is in principle a periodic signal of which the period should be measured, it makes perfect sense to use the Fourier Transform to obtain the fringe spacing (as done by Maeda et al. [2002]). However, this results in the amount of fringes per pixel F_{pix} , which then needs to

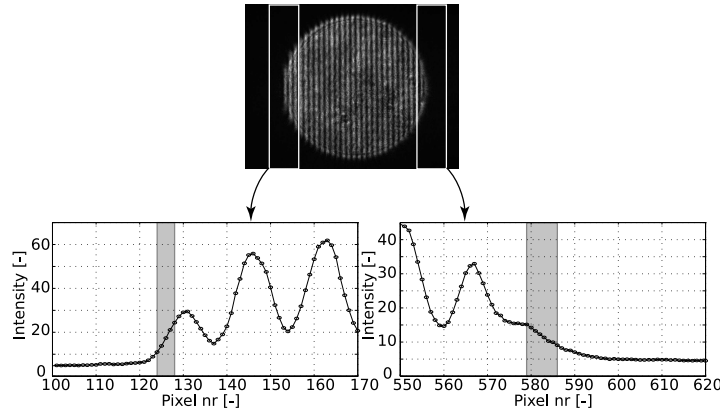


Figure 6: Ilids edge

be converted to radian. This calibration value is simply obtained by dividing the out-focus disc size expressed in pixels by its size in radian. The disc size in radian is equal to the collecting angle γ , which, in our case, is obtained from a numerical ray-tracing calculation of the measured optical set-up. The disc size in pixel Φ_{pix} follows from locating the edges of the out-focus disc in the intensity profile. Glover et al. [1995] already used this approach more or less since they determined the out-focus disc size with a Hough Transform and subsequent fitting. This leads to the following formula:

$$\frac{1}{\Delta\varphi} = F_{pix} \frac{\Phi_{pix}}{\gamma}$$

Note that this formula can be transformed into the previous one since $F_{pix}\Phi_{pix}$ is simply equal to the total amount of fringes in the disc N_f ! Thus, a fractional amount of fringes is obtained per bubble. However, this does not mean that this approach is per definition more accurate than fringe counting since the uncertainty is now spread over two terms. While the frequency determination with the Fourier Transform is expected to have a very small uncertainty, nothing has been said so far (to our knowledge) concerning the uncertainty related to the disc size determination. In order to quantify this error, a sample intensity profile (averaged over all rows) is shown in Figure 6. As can be seen, the disc edge is not discontinuous but smoothed significantly by diffraction. This leads to a fundamental uncertainty concerning the correct location of the edge. In the present case an uncertainty on the total disc size of 7 pixels must be allowed. This corresponds to an uncertainty of 1,5%. This value is by no means the average uncertainty but rather a lower bound as will be shown in Section 5.5 where the evolution of this value will be investigated for different parameters.

5.3 Theoretical Calibration

In Figure 6, one can already see on the zoom of the right edge that any computer program will have a very hard time to correctly detect the edge due to the fact that fringes continue to appear in the diffraction tails. Another problem which appears occasionally is the partial separation of the out-focus discs, resulting in similar oscillations in the edges. For this and other reasons it would be nice to calculate the expected disc size theoretically from the optical configuration. The traditional approach here is to use the thin lens approximation but this is not valid when using objectives (as the Micro-Nikkor 55mm lens in our experiments). Therefore, it is necessary to use the more general thick lens approximations. For details of the thick lens approximation we refer to Hecht [1990]. A simple derivation, based on the sketch of Figure 7, results in:

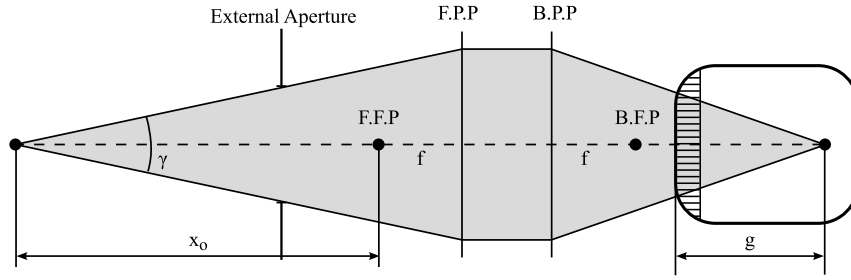


Figure 7: Thick lens approximation

$$\Phi_{pix} = \frac{2 \tan\left(\frac{\gamma}{2}\right) g x_o}{f S_{pix}}$$

Here, f is the focal length of the lens ($= 55$ mm), g is the out-focus distance of the ccd-plane, x_o is the distance from the object to the front focal plane and S_{pix} is the size of a pixel ($6,45 \mu\text{m}$). However, it is not the disc size that is needed, but the division of the disc size by the collecting angle. In this way we obtain a term $2 \tan\left(\frac{\gamma}{2}\right) / \gamma$. For moderate collecting angles, this term can be safely taken to be equal to 1 since the error for a collecting angle of 10° is only 0,25 %. Thus the fringe spacing for the theoretical case is:

$$\frac{1}{\Delta\varphi} = F_{pix} \frac{g x_o}{f S_{pix}} = F_{pix} \frac{g}{M S_{pix}}$$

where M is the magnification of the optical system. Note that this formula is not original and has appeared before (for instance Pan et al. [2005]). Nevertheless, the fact that this calibration value does not depend on the collecting angle is a very important one! This implies that this configuration does not require an accurate size and position measurement of the aperture as opposed to the experimental calibration. Therefore, the internal aperture of the objective can be used and the external one that is shown in Figure 1a can be removed. However, one of the important parameters in this case is g , the out-focus distance. While this can be measured in some configurations, it is not possible when an objective is used that is attached to the ccd-plane. Therefore, two special configurations will be introduced in section 5.5 which circumvent this problem elegantly.

5.4 Full Experimental Calibration

The last type of calibration is of course the full experimental calibration where the mapping of radian to pixel is determined experimentally by fitting the obtained result to the known diameter of a calibration target. This is, for instance, done by Pan et al. [2005] who measure the scattered pattern of an optical fiber placed at the measurement volume. Depending on the calibration target this can be indeed a very accurate calibration. Nevertheless, this is a rather difficult approach when measuring bubbles inside a closed reservoir.

5.5 Comparison of experimental and theoretical calibration

5.5.1 Camera focused at infinity

In this configuration, the objective is simply focused at infinity, a position that is always indicated clearly. In this state, the ccd-plane is located at the back focal plane of the lens. This implies that

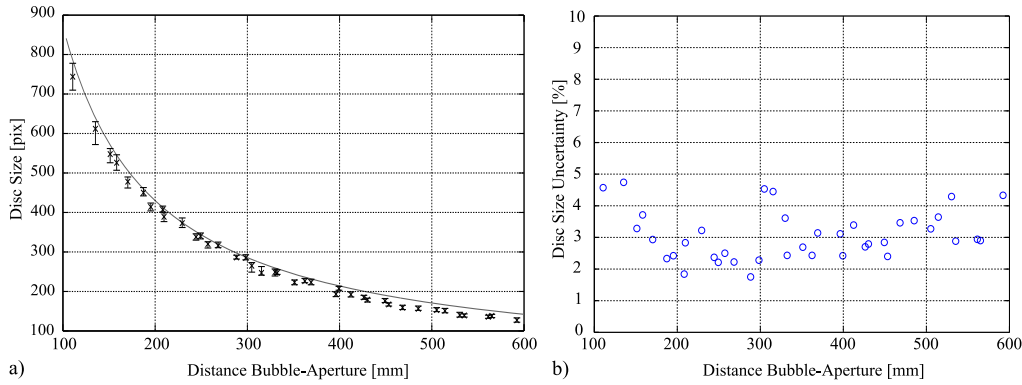


Figure 8: a) Experimental versus theoretical disc size for a camera focused at infinity b) Experimental disc size uncertainty

$g = x_i$ which simplifies the theoretical formula to:

$$\frac{1}{\Delta\varphi} = F_{pix} \frac{f}{S_{pix}}$$

which is an amazingly simple formula. Note that in this case, there is even no need to measure the location of the camera x_o ! Aside from its practical ease this also implies that there are almost no uncertainties left in this case. Both the focal length and the pixel size are values supplied by the vendor. In order to test the theory, the theoretical disc size was calculated and compared with the experimentally measured disc size for different positions of the camera along the rail on Figure 1a. The result of this comparison is shown in Figure 8a. While the correct trend is obviously captured by the theoretical continuous line, there is a substantial bias towards larger disc sizes. Analysis of this bias shows that the error is around 2% for the smallest stand-off distance and increases linearly up to 12% for larger distances. Since the uncertainty on the experimental disc size determination is approximately constant at 3% (Figure 8b), the error must come from the theoretical disc size calculation. In order to pinpoint the culprit, a sensitivity analysis was performed of the theoretical formula. This showed that an error of this magnitude could not be attributed to incorrect measurements of the collecting angle (which still plays a role in the theoretical *disc size* calculation). Additionally, a separate measurement of the focal length of the objective gave a result of 54,8 mm, which only introduces a bias of 0,36%. Finally, it was found that both the trend as the magnitude of the bias could be explained by assuming that the ccd plane is shifted by *only* 0,5 mm from the back focal plane! This can be appreciated from the theoretical disc size formula of section 5.3. In our case, the bias will be dominated by the error in g . Since g will decrease as the objective is placed further from the bubble, the procentual error $\frac{\Delta g}{g}$ will increase with distance as was observed in the experiment. This clearly shows that the theoretical configuration is extremely sensitive for this configuration, since a misplacement of 0,5 mm already results in errors of up to 12%.

Concerning the experimental calibration, we note that the uncertainty is approximately constant, independent of total disc size and stand-off distance. The average uncertainty was found to be close to 3%. To this, one needs to add the uncertainty on the collecting angle ($\pm 1\%$) in order to obtain the total calibration uncertainty of 4%.

5.5.2 Two-step calibration

One of the basic flaws of the previous configuration for a successful theoretical calibration was the decreasing out-focus distance as the camera is placed further away. The inverse approach however

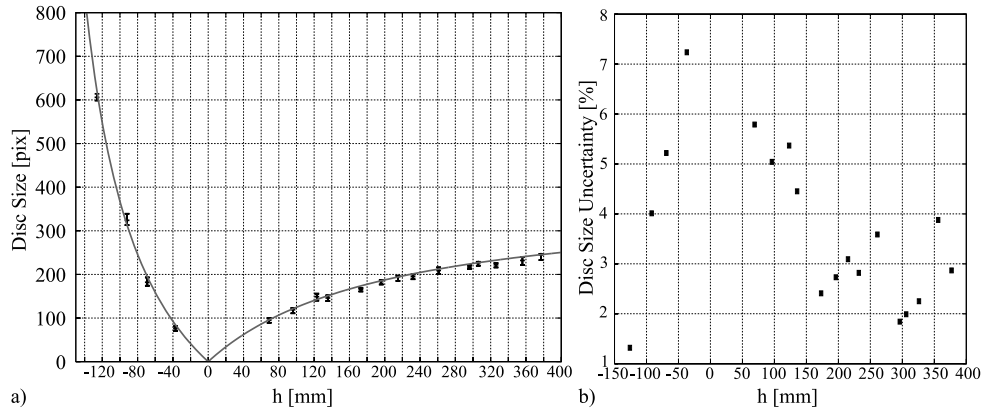


Figure 9: a) Comparison of theoretical and experimental disc sizes for the two-step calibration procedure b) Experimental uncertainty of the disc size determination

should result in decreasing uncertainties. This can be achieved by focusing the camera not at infinity but at its closest possible focus. Now, a two-step calibration as introduced in Pan et al. [2005] can be used in order to calculate the out-focus distance indirectly. In a first step the camera is focused at the target. Here, the distance $x_{o,if}$, being the distance from the front focal plane to the measurement volume, or the in-focus optical magnification M_{if} is measured. Then, the entire camera (ccd + objective) is displaced by an accurately measured amount h . This results in the following formula:

$$\frac{1}{\Delta\varphi} = F_{pix} \frac{fh}{x_{o,if} S_{pix}} = F_{pix} \frac{M_{if}h}{S_{pix}}$$

Again, this result was experimentally verified by comparing the theoretical and experimental disc sizes for different camera displacements h as shown in Figure 9a. With this procedure the theoretical and experimental results were in agreement. Concerning the uncertainty on the disc size determination; this reaches a peak close to the focusing position and decreases going further. However, when h approaches 300 the uncertainty stops decreasing and appears to remain constant afterwards at around 3% again. While this is not apparent from the graph, negative values of h were unsuited for ILIDS measurements since the discs did not overlap sufficiently.

5.6 Calibration conclusions

Counting fringes is by far the most inaccurate procedure to measure the diameter due to the impossibility to count accurately a fractional amount of fringes. This can be improved by performing an FFT-analysis but this has to be combined with a calibration of the amount of pixels per radian. As a general rule, one can say that the uncertainty on the experimental calibration is around 4% mostly due to diffraction effects and the ambiguity in locating the 'real' edge location. However, no experiments were performed with different objectives and different aperture locations and shapes so this value cannot be taken as a universal constraint on the precision of the experimental calibration procedure. A theoretical calibration can yield an improved calibration when the camera is placed on a close focus. With the described two-step calibration procedure, the main error sources are the determination of the in-focus optical magnification and the out-focus displacement of the entire camera h . In the present experiment, we obtained a variation of the magnification across the laser-sheet thickness of 0,6 %. In addition, when measuring at $h = 400\text{mm}$ with an estimated uncertainty on h of 1 mm, one needs to add a procentual uncertainty of 0,25 %. This leads to a combined uncertainty on the calibration of 0,65 %, which is a huge improvement over the experimental calibration. However, this could have

Table 1: Results for the comparison of different measurement techniques on the same bubble

backlighting	$0.608519 \pm 0.0917\text{mm}$
GPVS	$0.608625 \pm 0.0033 \text{ mm}$
ILIDS	$0.609933 \pm 0.0452 \text{ mm}$

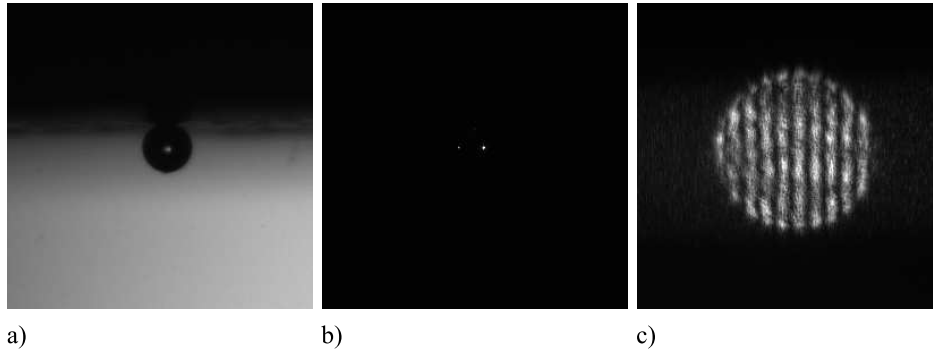


Figure 10: Comparison of a) backlighting b) GPVS and c) ILIDS measurements of the same bubble

been improved even more by considering the fact that the uncertainty on the in-focus magnification is really just due to the variation in $x_{o,if}$ across the laser-sheet thickness. Assuming for simplicity that $\Delta x_{o,if} = \Delta h$, this leads to an optimal configuration when $x_{o,if} = h$ since both uncertainties are equal then. Thus, for a given stand-off distance of the camera, the highest precision is obtained when the camera reaches a sharp focus half-way to the measurement volume.

However, these types of 'static' calibration, where the conversion is calculated before the measurements start, are not possible in cases where the disc size varies significantly for different positions in the laser-sheet. This is for example the case when one attempts to measure the third velocity component from the disc size. In this case, a combined theoretical and experimental procedure as performed by Grassmann and Peters [2004] can be used. Here, one first measures the disc size in pixels experimentally. This disc size is then placed in the theoretical disc size formulas to obtain the missing parameters as x_o and θ .

6 Comparison Backlighting-GPVS-ILIDS

Another advantage of our experimental set-up is that we are able to measure exactly the same bubble with ILIDS and any other technique. We chose to compare our ILIDS measurement with two other current 2D optical measurement techniques GPVS and backlighting. The three different images used are shown in Figure 10. Note that the ILIDS image was taken with parallel polarisation at an observation angle of 105° . This was done because GPVS is rather strict in the allowable observation angles and really needs two equally intense glare points.

The results of this comparison are shown in Table 1. We can see that all measurements were in excellent agreement with a procentual error between all the techniques that remained below 1 %. Concerning the associated uncertainties of the different techniques, we can note that the uncertainty of backlighting is the largest by far. This is due to diffraction which makes the task of finding the bubble edge very difficult and prone to errors. Next on the list is ILIDS. Note that this experiment was not yet performed with the suggested two-step calibration procedure and this would have reduced the uncertainty considerably. Finally, the highest precision is obtained with GPVS.

7 Discussion

When looking at the theoretical two-step calibration procedure, yet another similarity between GPVS and ILIDS is found. Both techniques need to measure the optical magnification of a calibration target. Thus, the common uncertainty sources for GPVS and ILIDS are the magnification and the conversion factor. To this one needs to add the frequency determination and the camera displacement for ILIDS and the glare point separation for GPVS. With the use of auto-correlation and similar techniques the uncertainty on GPVS measurements can be made very small, especially when telecentric lenses are used to decrease the magnification variation across the laser-sheet thickness. In comparison, ILIDS measurements have the additional requirement to measure the camera displacement as accurate as possible. However, while the size measurements might be of comparable precision, this is not the case for concentration and velocity measurements. This is due to the fact that not only the magnification changes when the camera is placed out-focus but there is also a translation of the objects. This was already mentioned by Damaschke et al. [2002] who noticed that a 2D calibration is needed to correlate the out-of-focus bubbles correctly with the in-focus images. This difficult calibration procedure will surely add to the total uncertainty on the concentration measurements since this decreases the accuracy of the location determination. Due to this uncertainty on the location determination, velocity measurements as well are not expected to be as precise than those with GPVS where standard PTV-techniques can be used. Of course, in ILIDS's defence one can state that one is able to measure micro-bubbles with standard lenses, a feat which is not possible with GPVS due to the high requirements on the optical magnification.

8 Conclusions

A new ILIDS configuration for measuring bubbles is introduced. Due to the presence of a known frequency signature this configuration is more robust than other present configurations. Next to this, a high precision two-step calibration procedure was also described. Finally, measurements of the same bubble were compared for three different techniques, i.e. backlighting, ILIDS and GPVS and these results were in excellent agreement.

Acknowledgements

We would like to thank D. Biondani and R. Prete for the help during our experiments. This research was funded with fellowship SB-031241 granted by the Flemish Institute for the Promotion of Scientific and Technological Research in the Industry (IWT).

References

- N. Damaschke, H. Nobach, T.I. Nonn, N. Semidetnov, and C. Tropea. Size and Velocity Measurements with the Global Phase Doppler Technique. In *11th international symposium on application of laser techniques to fluid mechanics*, Lisbon, 2002.
- S. Dehaeck, J. P. A. J. van Beeck, and M. L. Riethmuller. Extended glare point velocimetry and sizing for bubbly flows. *Experiments in fluids*, 39(2):407–419, August 2005.

- S. Dehaeck, J.P.A.J. van Beeck, and M.L. Riethmuller. Glare Point Velocimetry and Sizing (GPVS): Introduction of a new optical 2D measuring technique for bubbly flows. In *12th International Symposium on Application of Laser Techniques to Fluid Mechanics*, Lisbon, 2004.
- A.R. Glover, S.M. Skippon, and R.D. Boyle. Interferometric laser imaging for droplet sizing: a method for droplet-size measurement in sparse spray systems. *Applied Optics*, 34:8409–8421, 1995.
- A. Grassmann and F. Peters. Size measurement of very small spherical particles by mie scattering imaging (msi). *Part. Part. Syst. Charact.*, 21:379–389, 2004.
- Hecht. *Optics*. Addison Wesley, 1990.
- G. Koenig, K. Anders, and A. Frohn. A new light-scattering technique to measure the diameter of periodically generated moving droplets. *Journal of Aerosol Sciences*, 17:157–167, 1986.
- D.S. Langley and P.L. Marston. Critical-angle scattering of laser light from bubbles in water: measurements, models, and application to sizing of bubbles. *Applied Optics*, 23(7):1044–1054, April 1984.
- M. Maeda, Y. Akasaka, and T. Kawaguchi. Improvements of the interferometric technique for simultaneous measurement of droplet size and velocity vector field and its application to a transient spray. *Experiments in Fluids*, 33:125–134, 2002.
- Y. Niwa, Y. Kamiya, T. Kawaguchi, and M. Maeda. Bubble sizing by interferometric laser imaging. In *10th International Symposium on Application of Laser Techniques to Fluid Mechanics*, Lisbon, 2000.
- V. Palero, J. Lobera, and M. P. Arroyo. Digital image plane holography (diph) for two-phase flow diagnostics in multiple planes. *Experiments in Fluids*, 39(2):397–406, Aug 2005.
- G. Pan, J. Shakal, W. Lai, R. Calabria, and P. Massoli. Simultaneous global size and velocity measurement of droplets and sprays. In *Proceedings of the 20th ILASS - Europe Meeting*, 2005.
- R. Ragucci, A. Cavaliere, and P. Massoli. Drop sizing by laser light scattering exploiting intensity angular oscillation in the mie regime. *Part. Part. Syst. Charact.*, 7:221–225, 1990.
- N. Semidetnov and C. Tropea. Conversion relationships for multidimensional particle sizing techniques. *Measurement Science and Technology*, 15:112–118, 2004.